

Electrical and optical properties of PbTe *p-n* junction infrared sensors

A. S. Barros, E. Abramof,^{a)} and P. H. O. Rappl

Laboratório Associado de Sensores e Materiais (LAS), Instituto Nacional de Pesquisas Espaciais (INPE), CP 515, São José dos Campos, São Paulo 12245-970, Brazil

(Received 18 August 2005; accepted 29 November 2005; published online 20 January 2006)

Lead telluride mesa diodes were fabricated from a series of *p-n* junctions grown on (111) BaF₂ substrates, in which the hole concentration *p* was kept constant at 10¹⁷ cm⁻³ and the electron concentration *n* varied between 10¹⁷ and 10¹⁹ cm⁻³. Capacitance-voltage analysis showed that for *n* > 10¹⁸ cm⁻³ the PbTe *p-n* junction is one sided and abrupt. The parameters (incremental resistance, series and parallel resistances, and ideality factor) obtained from the current-voltage (*I-V*) characteristics and the detectivity *D*^{*} exhibited a large fluctuation among the photodiodes. In spite of these fluctuations, it was possible to correlate the noise and *D*^{*} values to the parameters obtained from the *I-V* analysis. These results allow predicting the PbTe detector's figures of merit from the data obtained from the *I-V* curves. The best PbTe photodiodes fabricated here showed *D*^{*} values close to 10¹¹ cm Hz^{1/2} W⁻¹, comparable to InSb and HgCdTe commercial detectors and to PbTe sensors fabricated on Si substrates. © 2006 American Institute of Physics.

[DOI: 10.1063/1.2161802]

I. INTRODUCTION

Narrow-band-gap semiconductors are appropriate materials for photon infrared detectors.¹ Lead telluride, due to its energy gap of 0.19 eV at 77 K, is an alternative candidate for detection applications in the 3–6 μm midwavelength infrared region. The PbTe photovoltaic infrared sensors are normally made from epitaxial layers grown on BaF₂ substrates or on Si substrates using fluoride intermediate layers. If the narrow gap material is grown directly on a Si substrate which contains the readout circuit, a monolithically integrated detector array can be accomplished. The fabrication of two-dimensional monolithic PbTe infrared sensor focal plane arrays for thermal imaging applications has been demonstrated.^{2–5} To simplify the fabrication process, the PbTe photovoltaic infrared detectors are usually produced from Schottky barriers using Pb blocking contacts deposited on a *p*-type PbTe layer with hole concentration in the low 10¹⁷ cm⁻³ range.^{2–4} Lead telluride *p-n* junctions have recently attracted attention as infrared detectors.^{6–8} In this case, an *n*⁺ (high 10¹⁸ cm⁻³) layer is grown on top of a *p*-type (~10¹⁷ cm⁻³) PbTe layer and mesa structures are etched to delineate the devices.^{7,8} Both types of PbTe infrared detectors showed comparable device performance.

Since the detector performance is strongly influenced by the characteristics of the *p-n* junction, it is desirable to know how the carrier concentration of the constituent layers influences the device properties. In this work, we investigate the electrical and optical characteristics of PbTe *p-n* junctions as a function of the electron concentration. For this purpose, we grew a series of lead telluride *p-n* junctions by molecular-beam epitaxy (MBE) on (111) BaF₂ substrates, in which the hole concentration *p* was kept constant at 10¹⁷ cm⁻³ and the electron concentration *n* ranged from 10¹⁷ to 10¹⁹ cm⁻³. The

carrier concentration of the PbTe layers was controlled by deviation from stoichiometry and extrinsic bismuth *n*-type doping. Mesa diodes were fabricated by lithographic methods and assembled in a LN₂ cryostat for characterization.

Dedicated automatic measurement systems for capacitance versus voltage (*C-V*) and current versus voltage (*I-V*) characteristics were employed for this work. *C-V* and *I-V* curves were measured at 80 K for diodes produced from the different *p-n* junctions. The *C-V* analysis allowed the determination of the junction type and depletion width. The diode parameters, obtained from the derivative of the *I-V* curves and from a simulation program developed to adjust the curve calculated by the equation for a real diode to the experimental data, were correlated to the noise voltage and detectivity values measured in an infrared optical bench.

II. DIODE FABRICATION

All samples were grown on freshly cleaved (111) BaF₂ substrates by molecular-beam epitaxy in a Riber 32P MBE apparatus equipped with effusion cells containing PbTe, Te, and Bi₂Te₃ solid sources. The beam equivalent pressure originating from each effusion cell was measured separately in a Bayer-Alpert flux monitor and was used as the main growth parameter. The growth conditions were evaluated *in situ* using a 12 keV reflection high-energy electron-diffraction system. During this experiment, the PbTe flux was kept at about 7 × 10⁻⁷ Torr and the substrate temperature at 300 °C, leading to a growth rate of 2.2 Å/s. Before properly growing the *p-n* junctions, PbTe reference layers were grown on BaF₂ substrates in order to determine the best MBE conditions to obtain both types of conduction at the intentional carrier concentration. The resistivity, carrier type and concentration, and mobility of the reference layers were measured at 300 and 77 K in a Hall-effect system with an electromagnetic field of 0.7 T.

^{a)} Author to whom correspondence should be addressed; electronic mail: abramof@las.inpe.br

TABLE I. Electrical data of the different types of PbTe p - n junctions grown by MBE. The carrier concentration (p/n), resistivity (ρ), and mobility (μ) are from Hall measurements performed on the reference layers at 77 K. The p -layer data are $p=1.8 \times 10^{17} \text{ cm}^{-3}$, $\rho=3.6 \times 10^{-3} \text{ } \Omega \text{ cm}$, and $\mu=9.6 \times 10^3 \text{ cm}^2/\text{v s}$.

Sample	Type	n (cm^{-3})	ρ ($\Omega \text{ cm}$)	μ ($\text{cm}^2/\text{v s}$)
D4005	p - n^{++}	3.6×10^{19}	7.2×10^{-5}	2.4×10^3
D4012	p - n^{++}	3.6×10^{19}	7.2×10^{-5}	2.4×10^3
D4007	p - n^+	3.0×10^{18}	2.5×10^{-3}	8.3×10^2
D4010	p - n	1.9×10^{17}	3.3×10^{-3}	1.0×10^4
D4022	p - n	9.6×10^{16}	3.4×10^{-3}	1.9×10^4

Since the deviation from stoichiometry controls the carrier character of the lead salts, our MBE $\text{Pb}_{1-y}\text{Te}_y$ solid source is intentionally prepared metal rich ($y=0.495$). Using this source, an n -type PbTe layer with an electron concentration of about $5 \times 10^{16} \text{ cm}^{-3}$ is normally grown at the usual substrate temperature of 300 °C without any additional Te flux. In order to obtain the p -type layer, the additional Te flux is increased until the character transition from n to p occurs. An extra Te flux of about 8×10^{-9} Torr is necessary in these growth conditions to change the carrier type. Hence, both p - and n -type PbTe layers with carrier concentration in the range of 10^{17} cm^{-3} could be obtained by playing with the stoichiometric deviation in the MBE system. However, to achieve higher electron concentration, the PbTe layers must be doped extrinsically. Bismuth, through the Bi_2Te_3 effusion cell, is normally used as an n -type dopant. A detailed study of Bi doping of PbTe layers in our MBE system was previously done.⁹ Using this work as a reference, we have determined the Bi_2Te_3 flux necessary to grow PbTe layers with the planned electron concentration in the range of 10^{17} , 10^{18} , and 10^{19} cm^{-3} .

After this calibration procedure, a series of p - n junction samples were produced. To form the junctions, a 3–4- μm -thick p -type layer is firstly grown on top of the BaF_2 substrate followed by an n -type layer of approximately 2 μm . For identification, the junctions with electron concentration in order of 10^{17} , 10^{18} , and 10^{19} cm^{-3} were named p - n , p - n^+ , and p - n^{++} , respectively. Table I displays the electrical data of all p - n junctions grown for this work, as determined from Hall measurements made on the reference layers at 77 K.

The diodes were fabricated through the etching of mesa structures and metallic contact depositions using lithographic processes. A stainless-steel mask containing circular holes with diameters of 1.0 and 0.3 mm was used to deposit Au disks on top of the n -type layer. An electron-beam source was used to evaporate gold and the film thickness was controlled by a quartz-crystal monitor until it reaches 200 nm. The thickness of the Au disks measured in an Alpha Step profile meter was actually 170 ± 5 nm. These disks were used as protective masks for the etching process as well as metallic contacts. Mesas were etched using a $\text{Br}_2:\text{HBr}:\text{H}_2\text{O}$ (1:40:40) solution until the p -type layer was reached. Another stainless-steel mask was used to deposit Au pads in the surround of each mesa structure to form the diode. Each $15 \times 15 \text{ mm}^2$ BaF_2 wafer contains nine diodes with the two

different mesa diameters. Gold wires were soldered to both Au pads with indium. The diode was mounted on a Cu plate and assembled in a LN_2 cryostat for both electrical and optical characterizations. The setup allowed back-side illumination with a cold shield which defined a field of view equal to 30°. The mesa diodes with diameter of 0.3 mm (1.0 mm) and area of $7.07 \times 10^{-4} \text{ cm}^2$ ($7.85 \times 10^{-3} \text{ cm}^2$) are named with a termination $P(G)$.

III. DEVICE CHARACTERIZATION

A. Capacitance versus voltage characteristics

The C - V characteristic of the produced diodes was measured with a HP4280A capacitance meter. The capacitance is measured through an alternate signal of 10 or 30 mV in a frequency of 1 MHz applied together with the dc voltage. The maximum capacitance measurable in this equipment is 2 nF. Due to the high dielectric constant of PbTe ($\kappa=800$ at 77 K), the diodes with 0.3 mm of diameter were designed in order to not overpass this value.

Figure 1 shows the inverse of the specific capacitance squared ($1/C^2$) versus the reverse voltage measured at 80 K, where C is the capacitance per unit area, for three p - n junctions with different electron concentrations. Observe that, for the diode fabricated from a p - n PbTe junction (p and $n \sim 10^{17} \text{ cm}^{-3}$) shown in the lower panel, the $1/C^2$ - V plot presented a complete non linear behavior, which indicates that the depletion region extends to both sides of the junction. In the other hand, for the p - n^+ ($n \sim 10^{18} \text{ cm}^{-3}$) and p - n^{++} ($n \sim 10^{19} \text{ cm}^{-3}$) junctions, the $1/C^2$ - V plot exhibited a linear behavior, as demonstrated by the linear fit (solid lines) in the middle and upper panels of Fig. 1. This result evidences that for electron concentration higher than 10^{18} cm^{-3} , a one-sided abrupt PbTe junction is formed with the depletion region located practically at the p side. For this type of junction, the p concentration can be determined from the slope of the $1/C^2$ - V plot, and the depletion width w as a function of applied voltage can be estimated from the C - V characteristic. Table II summarizes the parameters obtained from the C - V characterization performed on the diodes fabricated from the p - n^+ and p - n^{++} junctions. A hole concentration of $1.1 \times 10^{17} \text{ cm}^{-3}$ was found for the diodes fabricated from the p - n^+ junction, a value very close to $p=1.8 \times 10^{17} \text{ cm}^{-3}$ obtained for the reference layer by Hall-effect measurement (see Table I). In case of diodes fabricated from the p - n^{++} junctions, a lower value of p concentration at about $3 \times 10^{16} \text{ cm}^{-3}$ was found. This fact indicates that bismuth interdiffusion may start to take place for PbTe junctions with electron concentration as high as 10^{19} cm^{-3} . The depletion width for the p - n^+ and p - n^{++} junctions at $V=0$ were close to 1 μm . This value agrees with published data for PbTe p - n^+ diodes grown on Si substrates.⁷

B. Current versus voltage characteristics

To measure the current versus voltage (I - V) characteristic of the diodes, a dedicated system composed of a programmable power supply (Keithley 220), an ammeter (Keithley 2010), and a voltmeter (Keithley 199) was employed using a special cable assembly which guarantees accurate measure-

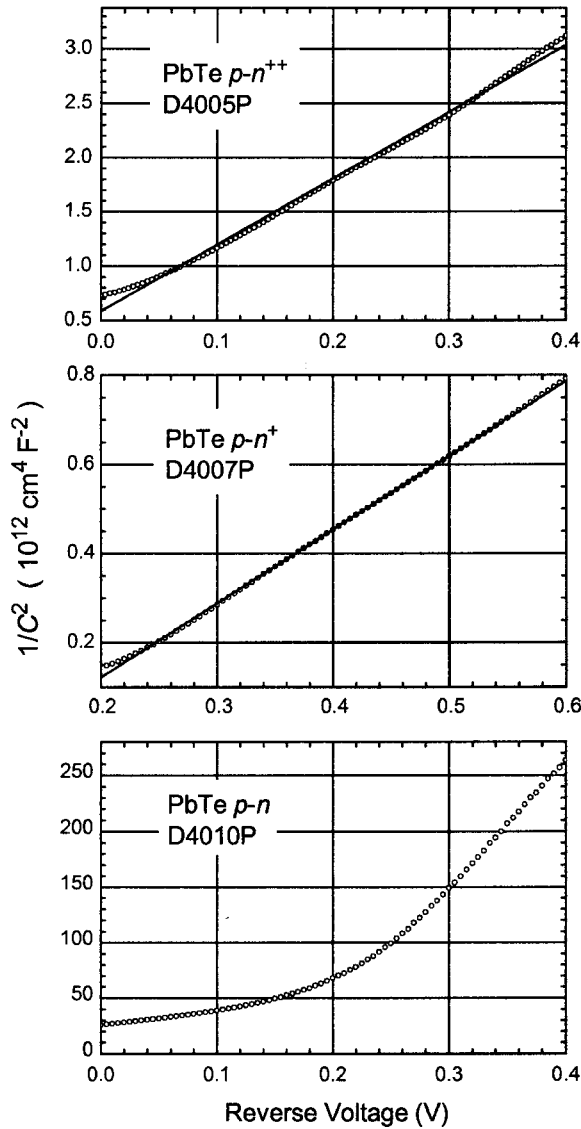


FIG. 1. $1/C^2$ - V plot for PbTe diodes at 80 K fabricated from p - n ($n \sim 10^{17} \text{ cm}^{-3}$), p - n^+ ($n \sim 10^{18} \text{ cm}^{-3}$), and p - n^{++} ($n \sim 10^{19} \text{ cm}^{-3}$) junctions. The solid lines are linear fits.

ment of the voltage drop across the junction and of the actual current flow. The I - V curves of commercial Si diodes were used to test and calibrate the system.

Figure 2 shows, as an example, the I - V characteristic of a PbTe diode fabricated from a p - n^{++} junction. In this case, the diode presented a nice I - V curve with a low leakage current in the reverse branch and a small series resistance in

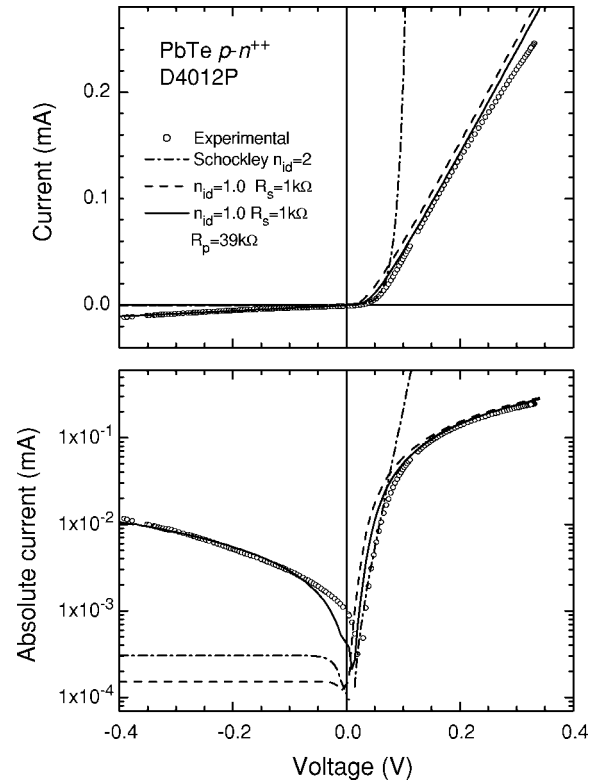


FIG. 2. I - V characteristic measured at 80 K for a PbTe diode from a p - n^{++} junction, which presented a low leakage current. The open circles correspond to the experimental data. The dashed-dotted line is calculated using Schockley equation with $n_{id}=2$, the dashed line is a fitting considering only R_s and n_{id} , and the solid line is the best fit considering all three parameters n_{id} , R_s , and R_p . The lower panel shows, in the ordinate, the modulus of the current in a logarithmic scale to improve visualization.

the forward direction. We have observed, contrarily to the C - V results, that the I - V curves exhibited different formats and values among all measured diodes. Even for diodes fabricated from the same wafer, different shapes were observed for both direct and reverse branches. The leakage current and the series resistance presented a significant variation among the diodes. Figure 3 shows, as an illustration, the I - V curve of a diode, which exhibits a large leakage current, produced from a p - n^+ junction.

In order to calculate the PbTe I - V curves and try to obtain quantitative information about the junctions, we used the following equation for a real diode:¹⁰

$$I = I_0 \left[\exp\left(\frac{V - IR_s}{n_{id} V_{th}}\right) - 1 \right] + \frac{V - IR_s}{R_p}, \quad (1)$$

which is an ideal diode together with a series R_s and a parallel R_p resistance. In this equation, n_{id} is the ideality factor, $V_{th} = k_B T / e$ is the thermal voltage at the measurement temperature T , and k_B and e are the Boltzmann constant and the electron charge, respectively. The saturation current $I_0 = n_{id} V_{th} / R_0$ can be determined using the incremental differential resistance $R_0 = (dV/dI)_{V=0}$, which can be easily obtained by differentiating the measured I - V curve. The above equation can only be solved numerically. Considering an infinite parallel resistance, the equation begins to have an analytical solution by isolating the terms relative to the voltage V . In this case, only the effects of the series resistance and

TABLE II. Hole concentration p and depletion width w as obtained from the C - V characterization on the diodes fabricated from p - n^+ and p - n^{++} junctions.

Diode	Type	p (cm^{-3})	w^a (μm)	w^b (μm)
D4005P	p - n^{++}	2.9×10^{16}	0.60	1.25
D4012P	p - n^{++}	2.3×10^{16}	1.93	2.28
D4007P	p - n^+	1.1×10^{17}	0.27 ^c	0.48

^a $V=0$.

^b $V=-0.4$ V.

^c $V=-0.2$ V.

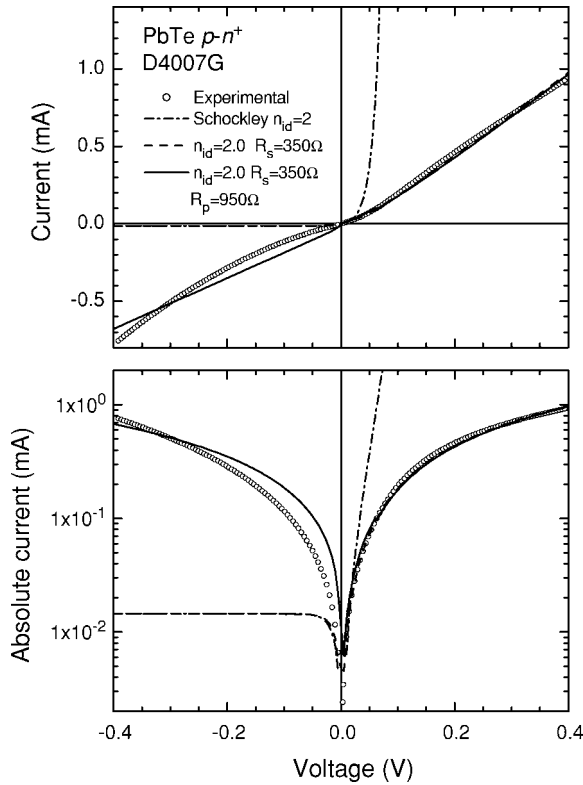


FIG. 3. Same as in Fig. 2 for a PbTe diode, which showed a large leakage current, fabricated from a $p-n^+$ junction.

the ideality factor are considered. For a null R_s and an infinite R_p , the equation reduces to the Shockley equation of an ideal diode.

Besides the experimental $I-V$ values shown in open circles, the graphs in Figs. 2 and 3 also plot the calculated curves. The dash-dotted lines are calculated using the Shockley equation with $n_{id}=2$. The dashed lines are the fits considering only the series resistance and the ideality factor. Note that the series resistance fits the direct branch of the $I-V$ curve. The solid lines are the best fit considering all three parameters n_{id} , R_s , and R_p . Observe that R_p influences mainly the branch of the reverse voltage. For a better visualization, the lower panels of Figs. 2 and 3 show in the ordinate the modulus of the current in a logarithmic scale. It is important

to mention that we were able to fit simultaneously both sides of the $I-V$ curve using the above real diode equation.

The parameters obtained from this fitting procedure applied to all measured diodes are displayed in Table III. The results show a reasonable fluctuation in the parameters of the diodes. The incremental differential resistance varied between 0.32 and 45 k Ω and the R_0A product, where A is the photodiode area, from 0.23 to 31.8 Ω cm². The series resistance varied from 35 to 1100 Ω , while R_p ranged from 0.63 to 39 k Ω . Due to this variation, it was not possible to find any correlation between the parameters obtained from the $I-V$ curves and the electron concentration in the $p-n$ junction. The ideality factor for the different diodes varied between 1.0 and 4.0. For a conventional diode, n_{id} has a value between 1 and 2 depending if the diffusion or the recombination current is dominant. If n_{id} values higher than 2 are found, other mechanisms of current injection may be present in the diodes. Superficial currents at the mesa edges (leakage currents) are the main extra injection mechanism, which normally contribute to undesirable noise in the photovoltaic detectors. Ideality factors higher than 2 were also observed for PbTe $p-n$ junctions^{6,8} and for Pb/PbSnSe Schottky barriers.¹¹ We believe that this large variation observed among the diodes is due to nonuniformities during the diode processing and the absence of a passivation layer.

C. Detectivity measurements

In order to determine the performance of the fabricated devices as infrared photovoltaic detectors, the detectivity of all PbTe photodiodes was measured at 80 K in an infrared optical bench. To perform this measurement, the radiation from a blackbody source at $T=900$ K, chopped with a frequency of 900 Hz, illuminates the detector through the cryostat BaF₂ window. A power density $H=5.65 \times 10^{-4}$ W cm⁻² reaches the detector and the root-mean-square voltage signal V_S is measured in a lock-in amplifier with a bandwidth $\Delta f=14$ Hz. The detector noise V_N was measured for a background at 300 K and a field of view of 30°. The integral detectivity D^* is then calculated by the following relation:

TABLE III. Data obtained from the $I-V$ characterization of the photodiodes: incremental differential resistance R_0 , R_0A product, ideality factor n_{id} , series resistance R_s , and parallel resistance R_p . The integral detectivity D^* of each diode is also displayed.

Diode	Type	R_0 (k Ω)	R_0A (Ω cm ²)	n_{id}	R_s (Ω)	R_p (k Ω)	D^* (cm Hz ^{1/2} W ⁻¹)
D4005P	$p-n^{++}$	0.91	0.64	4.0	140	0.63	5.96×10^8
D4005G	$p-n^{++}$	0.57	4.48	4.5	35	0.45	4.47×10^8
D4012P	$p-n^{++}$	45.0	31.8	1.0	1000	39.0	8.01×10^{10}
D4012G	$p-n^{++}$	1.72	13.5	4.5	450	1.90	4.47×10^9
D4007P	$p-n^+$	1.80	1.28	3.6	370	1.30	2.74×10^8
D4007G	$p-n^+$	0.95	7.43	2.0	350	0.95	5.93×10^8
D4010P	$p-n$	0.32	0.23	2.0	200	0.70	1.41×10^8
D4010G	$p-n$	2.00	15.7	1.0	900	3.50	1.64×10^{10}
D4022P	$p-n$	6.97	4.93	3.1	600	19.0	2.31×10^{10}
D4022G	$p-n$	1.06	8.35	1.0	1100	4.20	1.52×10^9

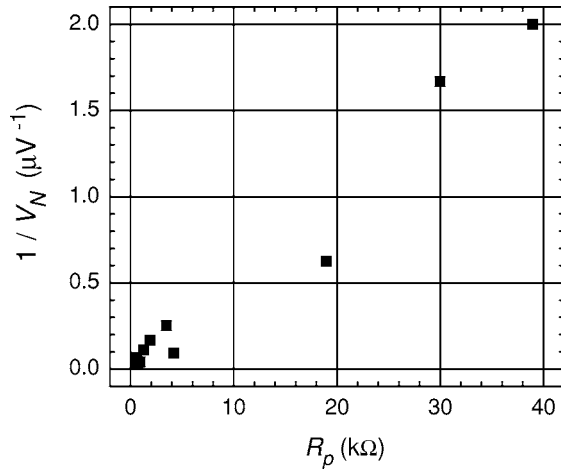


FIG. 4. Inverse of noise voltage V_N as a function of parallel resistance R_p for the PbTe photodiodes.

$$D^* = \frac{1}{H} \sqrt{\frac{\Delta f V_S}{A V_N}}. \quad (2)$$

The D^* values for all measured diodes is displayed in Table III. Like the parameters from the I - V curves, the detectivity also showed a large fluctuation among the different diodes, it varied from 1.4×10^8 to 8.0×10^{10} $\text{cm Hz}^{1/2} \text{W}^{-1}$.

The spectral response was measured in the same system as for the detectivity, by placing a grating monochromator between the infrared source (Glowbar) and the detector. The spectral response of the infrared sensor under test is compared to the one of a piroelectric reference detector. A cutoff wavelength of $5.9 \mu\text{m}$, corresponding to the energy gap of PbTe, was observed for all devices.

IV. CORRELATION BETWEEN ELECTRICAL AND OPTICAL MEASUREMENTS

In order to correlate the diode parameters determined from the I - V characterization to the detectivity measurements, some analyses are performed here. Figure 4 shows the inverse of the noise voltage V_N , measured with the preamplifier, as a function of the parallel resistance R_p . One can clearly see an inverse relation between V_N and R_p , i.e., smaller leakage currents (higher R_p) lead proportionally to lower noise in the infrared detector. This fact reflects directly in the detectivity, as can be confirmed in the graph of Fig. 5, where D^* is plotted as a function of R_p . Note that for $R_p > 10 \text{ k}\Omega$, integral detectivity values higher than $10^{10} \text{ cm Hz}^{1/2} \text{W}^{-1}$ are achieved for our PbTe infrared detectors.

Figure 6 plots the D^* values as a function of the R_0A product for the PbTe photodiodes at 80 K. Despite some fluctuations, the graph shows the expected tendency of increasing detectivity with increasing R_0A values. Note that the relation $D^* \sim (R_0A)^{1/2}$ is not observed in this graph, since this relation is valid for detectors that show only the Johnson thermal noise. This fact indicates that other sources besides the thermal noise are present in our detectors. Leakage cur-

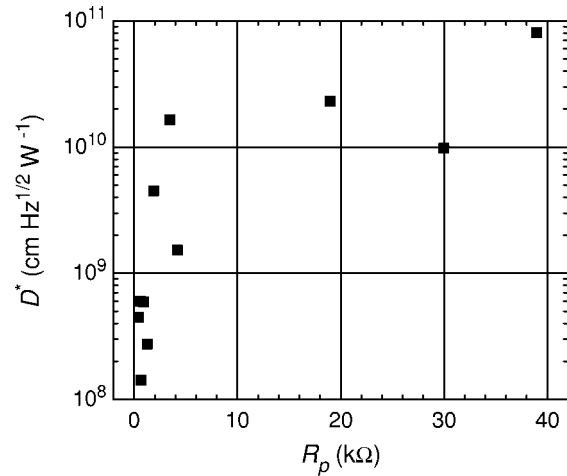


FIG. 5. Relation between the integral detectivity D^* and the parallel resistance R_p for the PbTe p - n junction infrared detectors.

rents at the mesa surface, as already observed during the I - V analysis previously described, are the main reason for the decrease in the detectivity values.

The highest values of R_0A product, measured for the PbTe photodetectors grown on BaF_2 substrates during this work, are close to the values found in the literature for PbTe p - n junction infrared sensors grown on Si substrates.⁶⁻⁸ It is important to remember that the R_0A values measured for PbTe diodes are always lower than the values obtained for InSb and HgCdTe photodiodes with equivalent cutoff wavelength.¹ In spite of this fact, comparable detectivities are found for the PbTe photodetectors. The threading dislocations typically present in the lead salts are responsible for the lower R_0A values observed in these materials. An inverse relation between R_0A product and the dislocation density was observed for lead salt photodiodes fabricated on silicon.^{3,7,8} It is important to emphasize that detectivity values D^* close to $10^{11} \text{ cm Hz}^{1/2} \text{W}^{-1}$ at 80 K, achieved for the best photodiodes fabricated here, are comparable to the ones of commercial InSb and HgCdTe infrared detectors with cutoff wavelength near to $6 \mu\text{m}$.¹

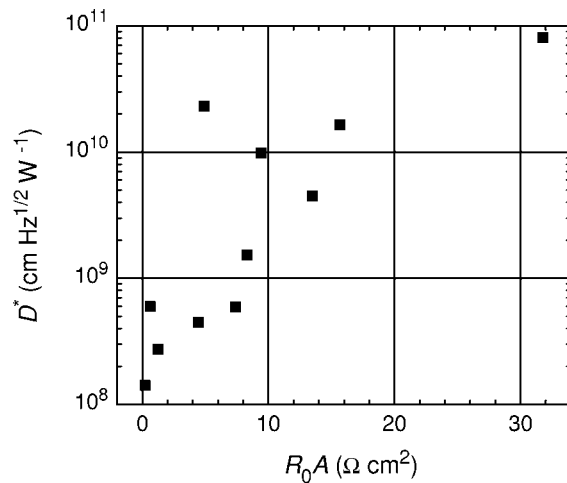


FIG. 6. Detectivity as a function of the R_0A product for our PbTe photodetectors.

V. CONCLUSIONS

A series of PbTe p - n junctions with different carrier concentrations were grown by MBE on (111) BaF₂ substrates. Mesa diodes were fabricated and mounted in a LN₂ cryostat for electrical and optical characterizations. Results from the C - V characteristic analysis revealed that a one-sided abrupt junction is formed for $n > 10^{18}$ cm⁻³. Depletion widths around 1 μ m were determined for these junctions. From the I - V measurements, the incremental differential resistance R_0 , the R_0A product, the series R_s and parallel R_p resistances, and the ideality factor n_{id} were determined for all diodes using the derivative of the curve and a best fit to the real diode equation. These parameters and the D^* values presented a large fluctuation among the different diodes. In spite of this variation, the parameters obtained from the I - V analysis could be well correlated to the noise voltage and D^* values. These results allow estimating the figures of merit of PbTe p - n junction sensors from the data derived from the I - V curves. The best PbTe photodetectors fabricated here showed detectivities comparable to the commercial InSb, HgCdTe, and PbTe on Si infrared detectors.

ACKNOWLEDGMENTS

The authors are very grateful to FAPESP (Project 00/112529-6), CNPq (Grant No. 300811/04-7), and CAPES for financial support.

- ¹A. Rogalski, *Infrared Phys. Technol.* **43**, 187 (2002).
- ²H. Zogg, A. Fach, C. Maissen, J. Masek, and S. Blunier, *Opt. Eng.* **33**, 1440 (1994).
- ³H. Zogg, *Proc. SPIE* **3629**, 52 (1999).
- ⁴H. Zogg, K. Alchalabi, D. Zimin, and K. Kellermann, *Infrared Phys. Technol.* **43**, 251 (2002).
- ⁵H. Zogg, K. Alchalabi, D. Zimin, and K. Kellermann, *IEEE Trans. Electron Devices* **50**, 209 (2003).
- ⁶C. Boschetti, P. H. O. Rappl, A. Y. Ueta, and I. N. Bandeira, *Infrared Phys.* **34**, 281 (1993).
- ⁷J. John and H. Zogg, *J. Appl. Phys.* **85**, 3364 (1999).
- ⁸D. Zimin, K. Alchalabi, and H. Zogg, *Physica E (Amsterdam)* **13**, 1220 (2002).
- ⁹A. M. P. Anjos, E. Abramof, P. H. O. Rappl, A. Y. Ueta, and H. Closs, *Braz. J. Phys.* **34**, 653 (2004).
- ¹⁰N. Veissid, D. Bonnet, and H. Richter, *Solid-State Electron.* **38**, 1937 (1995).
- ¹¹C. Paglino, A. Fach, J. John, P. Müller, H. Zogg, and D. Pescia, *J. Appl. Phys.* **80**, 7138 (1996).